Vol. 22, No. 3(2023) Proc231
Revista Mexicana de Ingeniería Química

Improvement of alkyd paints with NiO-ZrO_2Y coatings on hot-rolled steel

Mejoramiento de las pinturas alquídicas con recubrimientos de NiO-ZrO_2Y sobre acero HR

C. Cano, E. Romero, G.I. Cubillos*

Research Group on Chemical Materials and Processes, Departamento de Química, Universidad Nacional de Colombia, Av. Cra. 30 No 45-03, Bogotá-Colombia.

Received: April 17, 2023; Accepted: September 15, 2023

Abstract

The corrosion resistance of an alkyd paint was evaluated, substituting commercial anticorrosive with a thin film of nickel oxide zirconium oxide partially stabilized with Ytria (NiO-ZrO_2Y) deposited by means of the RF sputtering technique. Hot-rolled steel (HR) was used as the substrate. For the two anticorrosive coating systems, the structure, morphology, and composition were determined via the techniques of X-ray diffraction (XRD), scanning electron microscopy (SEM), energy-dispersive X-ray spectroscopy (EDX), and X-ray photoelectron spectroscopy (XPS) in order to determine the composition of the NiO-ZrO_2Y film. The corrosion resistance was determined from polarization curves and weight loss by immersion in a 3.5% NaCl solution. The electrochemical and weight loss results indicated that use of the NiO-ZrO_2Y film shows a fourfold increase in the corrosion resistance of the material subjected to immersion in the corrosive electrolyte compared to the traditionally-used commercial anticorrosive.

Keywords: Alkyd paint, NiO-ZrO_2Y coatings, corrosion under immersion, potentiodynamic polarization, EIS.

Resumen

Se evaluó la resistencia a la corrosión de una pintura alquídica, sustituyendo el anticorrosivo comercial por una película delgada de NiO-ZrO_2 parcialmente estabilizada con Ytria, depositada mediante la técnica de sputtering RF. Como sustrato se utilizó acero laminado (HR), tradicionalmente empleado a nivel doméstico e industrial. Para los dos sistemas de recubrimiento anticorrosivo, se determinó la estructura, morfología y composición mediante las técnicas de difracción de rayos X (DRX), microscopía electrónica de barrido (SEM), espectroscopía de energía dispersiva de rayos X (EDX) y espectroscopía de fotoelectrones de rayos X (XPS, para determinar la composición de la película de NiO-ZrO_2Y. La resistencia a la corrosión se evaluó a partir de las curvas de polarización lineal, espectroscopía de impedancia electroquímica (EIS) y pérdida de peso por inmersión en una solución de NaCl al 3,5%. Los resultados electroquímicos y de pérdida de peso muestran que el uso de la película de NiO-ZrO_2Y incrementa cuatro veces la resistencia a la corrosión del material sometido a inmersión en el electrolito corrosivo, en comparación con el anticorrosivo comercial utilizado tradicionalmente.

Palabras clave: Pintura alquídica, recubrimientos NiO-ZrO_2Y, corrosión, polarización potenciodinámica, EIS.

*Corresponding author. *E-mail*: gcubillos@unal.edu.co
https://doi.org/10.24275/rmiq/Proc231
ISSN:1665-2738, *issn-e*: 2395-8472

1 Introduction

Economic losses generated worldwide by the corrosion of metals are on the order of 4% to 8% of the GDP of both industrialized and developing countries. The process is of great importance on a domestic and industrial level and is much greater in geographical areas located near the sea, where the localized corrosion exerted by sodium chloride progresses much more rapidly (Barot *et al*., 2020; Shekari *et al*., 2017; X. Zhang *et al*., 2022). Equipment losses generated by pitting corrosion have direct repercussions in the form of economic losses and many times in human losses and will undoubtedly increase with climate change, which will trigger a rise in the sea level in coastal areas (Abdrabo *et al*., 2022; Mehvar *et al*., 2018; Tansel & Zhang, 2022; Y. Zhang *et al*., 2022). This effect of corrosion under immersion is also observed in geographical places where its inhabitants have to build their homes on the seashore, where the corrosion process is much more accelerated, as a last alternative, since they are in direct contact with the waves from the sea, undergoing a direct impact of sodium chloride in solution. This results in an accelerated deterioration of metals associated with construction and triggers large economic costs for low-income communities. Increasing the durability of a coating put into service contributes not only to counteracting the economic impact generated by the corrosion process, but also to cushioning the environmental impact produced by the continuous deterioration of paints (Kausley *et al*., 2018).

Associated with the corrosion process is the increase in environmental pollution, generated by the large number of metal parts with organic coatings that must be discarded (International Organization for Standardization, 2019). Alkyd paints, in particular, used as a binder in oil-based paint formulations, generate significant volumes of wastewater with high concentrations of organic compounds derived from phthalic acid and its esters (Kausley *et al*., 2018). Polymeric coatings are widely used for steel protection due to their relatively low cost and their versatility. Compared to epoxy paints developed for aggressive saline environments, with a cost 6 times higher than alkyd paints, the latter are the most widely ones used at home, even in saline and/or humid environments in developing countries (Asemani *et al*., 2016; Marsh *et al*., 2001). The use of alkyd paint leads to great economic losses, since the anticorrosive-alkyd paint system provides resistance to environments of only a medium corrosive category, due to its low adhesion (Alonso-Villar *et al*., 2021; Jin *et al*., 2020; Vorobel *et al*., 2021). In a saline or humid environment, the degradation process of this type of paint is accelerated by the formation of cracks and blisters, which is directly associated with the traditionally-used anticorrosive (Alonso-Villar *et al*., 2021; Araujo *et al*., 2010).

Studies related to the economic impact generated by losses due to corrosion are not enough to prevent it (Barot *et al*., 2020; Shekari *et al*., 2017); it is necessary to improve protection processes against corrosion in order to increase the life of the equipment put into service. Employing zirconia as an anticorrosive would be an alternative for improving metal-alkyd coating adhesion. It is known that ZrO_2 is characterized by its excellent properties of resistance to corrosion and that it can be synthesized by means of various methods(Joos *et al*., 2014; Roa *et al*., 2011; Talebi *et al*., 2010; Usseglio-Viretta *et al*., 2014). Zirconia deposited as a thin film on various types of steel has been shown to increase the corrosion resistance of the substrate (Cubillos *et al*., 2021; He *et al*., 2022; Tripathi *et al*., 2020), and as a buffer layer, it increases the corrosion resistance of epoxy paints (Asemani *et al*., 2016). The resistance to corrosion of a coating with zirconia varies according to the type of organic coating used (Asemani *et al*., 2016; Chen *et al*., 2018); however, the zirconia/alkyd paint system has not been studied, and therefore constitutes the aim of the present investigation.

In the present paper, we replaced the commercial anticorrosive layer with a nanometric film of zirconia partially stabilized withY^{3+}, Ni^{2+} in order to improve the adhesion between the alkyd paint and the substrate. It is known that zirconia is an excellent ceramic capable of protecting steels against corrosion in a saline environment (Cubillos *et al*., 2021; He *et al*., 2022; Tripathi *et al*., 2020) and that the incorporation of nickel into the coating generates micropores and increases its hardness and Young's modulus (Chen *et al*., 2018; Joos *et al*., 2014; Talebi *et al*., 2010; Usseglio-Viretta *et al*., 2014). These micropores could favor the diffusion of the organic coating in the zirconia layer and improve the adhesion with the ceramic. Thin films NiO-ZrO_2Y were deposited via the sputtering technique and subsequently covered with alkyd paint (ZAP system). The corrosion resistance of the ZAP system was evaluated by means of polarization curves and by direct immersion in a 3.5% NaCl solution at 29 °C. The corrosive process was determined on the basis of the percentage of mass loss, commonly used in the detection of general corrosion and pitting corrosion. The corrosion results obtained were compared with those of the commercial system: anticorrosive-alkyd paint (AAP system), traditionally employed for domestic use.

Table 1. Composition of hot-rolled steel.

Element	%	Element	%
Fe	99.507(2)	Sb	0.0140(44)
Mn	0.151(30)	Sn	0.0110(1)
C	0.1090(7)	Ta	<0.0100(6)
Si	0.0480(65)	P	0.0090(5)
N	0.0400(1)	B	0.0090(1)
Ti	0.0250(6)	Nb	<0.007
As	0.0230(7)	Al	0.0061(2)
V	0.0200(3)	S	0.0020(8)
Se	0.0160(48)	Ca	0.0012(2)
Wo	0.015(6)		

2 Experimental

2.1 Substrate preparation and coatings

For the substrate, HR steel specimens with dimensions of 26×26×3 mm were used, and their chemical composition is presented in Table 1. All the samples were polished with 120, 220, 340, 400, and 600 grit silicon carbide. Subsequently, they were washed with anionic surfactant and dried in air, and the organic residues were removed by washing with isopropanol in ultrasound equipment. The NiO-ZrO_2Y coating was deposited by sputtering from a nickel target supported on a zirconia target partially stabilized with yttria. For the AAP system, a commercial anticorrosive and a commercial alkyd paint for metal was used. For the ZAP system, the same alkyd paint was used on the zirconia deposited using RF sputtering.

2.1.1 Sputtering coatings

HR steel polished up to 600 grits was coated via sputtering using an Alcatel HS 2000 model. A base pressure of 4×10^{-5} mbar was used, with working pressure 7.4×10^{-3} mbar. Plasma was generated from 99.999% high-purity argon with a flow of 25.0 sccm. The power applied to the target was 250W, and the deposition temperature 115 °C for 45 minutes.

2.1.2 Alkyd paint coatings

The anticorrosive and alkyd paint were applied directly on the polished specimens using a brush. 3 layers of anticorrosive and three of paint were applied, with intervals of 6 hours of drying at room temperature between layers. Between each application, a 90º turn was given to the specimen to form a grid with the coating. In the specimens coated with zirconia only, 3 layers of the alkyd paint were applied.

2.2 Characterization

The crystalline structure of the coatings was determined via X-ray diffraction (XRD) using a PANanalitycal X'PERT equipment with Cu Kα radiation (0.154 nm). The X-ray source was operated at 45 kV and 40 mA, with a range of 10° to 90º 2Θ. The phases present in each of the samples were identified using the JCPDS database. The morphology was evaluated via scanning electron microscopy by means of a Quanta 2000 SEM, with X-ray dispersive energy spectroscopy (Bruker EDX). The elemental composition and the chemical bonds of the NiO-ZrO_2Y thin films were measured via X-ray photoelectron spectroscopy (XPS) using an AXIS Ultra DLD system (Kratos Analytical). The photoelectron spectra were excited by a soft X-ray Al Kα (1486.6 eV) anode at a power of 120 W (10 mA, 12 kV). The specimen was sputtered with Ar+ ions at 3 keV for 1 min to eliminate surface contamination. The C1s peak from the adventitious carbon-based contaminant with a literature value of 284.8 eV was used as a reference to calibrate the XPS spectra and eliminate the charging effect (Turner *et al*., 1993). The values of the binding energies (BE) are accurate to ±0.2 eV.

2.3 Evaluation of corrosion resistance

A cell with a configuration of three electrodes was used: Ag/AgCl reference electrode (0.197 mV/SHE), a working electrode (the coated HR-steel test piece with an exposed area of 1.00 cm^2), and a counter electrode (graphite). As a corrosive electrolyte, a 3.5% NaCl solution was used. A Princeton Applied Research model Versastat 4 potentiostat was used. In each test, 3 h of open circuit potential (Eoc) was measured with the objective of letting the corrosion potential stabilize. Subsequently, EIS measurements were performed in potentiodynamic mode with a perturbation voltage of 20 mV vs. the corrosion potential. The signal amplitude was 10 mV rms, and the measurement frequency ranged from 105 to 10^{-2} Hz. Three repeated tests were performed for each set of measurements in order to ensure the reproducibility of the results. Potentiodynamic polarization tests were conducted by varying the potential between -1000 and 2000 mV of the corrosion potential (E_{corr}) at a rate

of 0.1667 mV s^{-1}. CorrView was employed to study the LP curves. The weight loss analysis was performed on a Tecator 1024 thermostatic shaking water bath in 3.5% NaCl at 29 °C, at 3 rpm, for 304 days, on the day on which the last of the test tubes failed. The weight loss was calculated with Equation (1).

$$\text{average percentage weight loss (\%)} = \frac{w_f - w_i}{w_i} \times 100\% \quad (1)$$

where w_f and w_i correspond to the final weight and initial weight, respectively.

3 Results and discussion

3.1 Crystal structure and chemical composition

In Fig. 1, the diffractogram for the uncoated HR steel and the NiO-ZrO_2Y film deposited on the same steel is presented. The X-ray diffraction profile for the steel shows characteristic signals at 2θ: 44.64, 64.95, and 82.26, corresponding to the planes with Miller index (110), (200), and (211) of Fe. For the NiO-ZrO_2Y film, four crystalline phases were identified from International Center for Diffraction Data (JCPDS) databases, Y_2O_3-*c* (00-039-1065), ZrO_2-*c* (00-003-0640), NiO-*c* Nickel Oxide (00-004-0835), and Fe_2O_3-*c* maghemite (00-004-0755). Yttria and zirconia were deposited from the zirconia target partially stabilized with yttria. The presence of NiO suggests the oxidation of the nickel deposited by the reaction in the solid phase, and the presence of maghemite reflects the oxidation of the substrate during the deposition time. Despite working in an inert atmosphere at very low pressure, it is difficult to eliminate all the residual oxygen from the sputtering chamber, and the HR steel is highly susceptible to oxidation, because of its thermodynamically more stable state ΔG Fe_2O_3= -742.2 KJ/mol. The diffractogram for the commercial anticorrosive was characterized by being amorphous.

Regarding the chemical composition determined via EDX, the results for the NiO-ZrO_2Y film showed signals at 0.156 and 2.048 eV, corresponding to Zr, and 0.5038 eV, characteristic of oxygen, and those observed at 0.829, 7.360, and 8.198 eV correspond to Ni, see Fig. 2, Table 2. No yttrium was observed, due to its low concentration in the coating, which suggests that it may be below the detection limit of the equipment. The iron corresponds to the substrate. Based on the percentages of Ni, Zr, and O, the composition of the film is predominantly made up of zirconia. However, XPS indicated that the chemical composition of the coating shows the presence of Ni^{2+}, Y^{3+}, and Zr^{4+}, presented in Fig. 3.

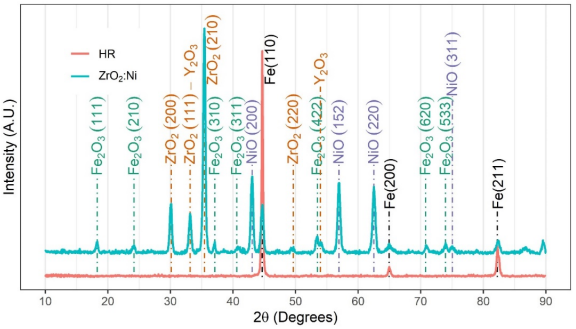

Fig. 1 XRD of HR steel and HR- NiO-ZrO_2Y.

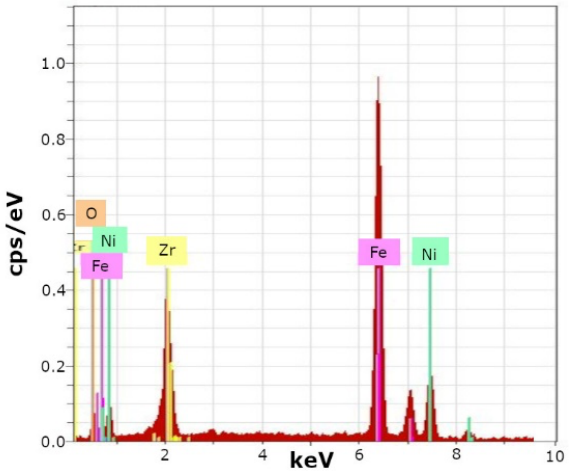

Fig.2 EDX coatings NiO-ZrO_2.

Table 2. Chemical composition of coatings Ni-ZrO_2Y.

Element	Chemical composition (wt %)
Zr	51.1
O	25.6
Ni	23.4

XPS analysis showed that the surface of the coatings was composed of the elements Ni^{2+}, Y^{3+}, Zr^{4+}, and O_2-. High-resolution XPS spectra of NiO-ZrO_2Y for Ni_{2p}, Zr_{3d}, Y_{3d}, and O_{1s} after cleaning with Ar^+ for 1 min are shown in Fig. 3. The binding energy at 853.0 and 870.2 eV was Ni^{2+} 2p in NiO (Bernasik *et al.*, 2002), the binding energy at 157.8 and 159.9 eV was identified for Y^{3+} 3d in Y_2O_3 (Gan *et al.*, 2018; Lei *et al.*, 2013, 2015), and signals centered at 182.4 eV and 184.0 doublet with a separation of 2.4 eV corresponds to the zirconium 3d in ZrO_2(Gan *et al.*, 2018). The core levels for oxygen were deconvoluted into two types of bonding according to the broadness and symmetry. The two peaks are located at 530.4 and 532.2 eV, corresponding to the Y-O Zr-O bond in Y_2O_3 and ZrO_2, and the signal at 532.2 eV physisorbed atmospheric H_2O (Lei *et al.*, 2013). These results confirm the presence of the previously-identified phases using DRX and identify the Y_2O_3 phase in the coating.

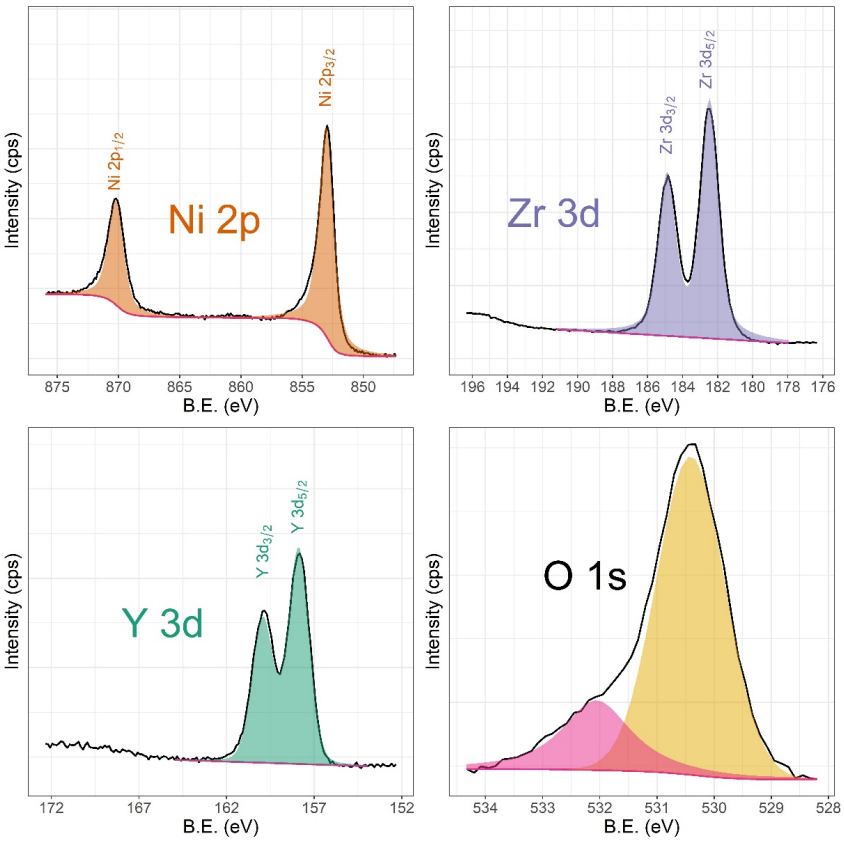

Fig. 3 High-resolution XPS spectra of NiO-ZrO_2Y for Ni 2p, Zr 3d, Y 3d, and O 1s after cleaning with Ar^+ for 1 min.

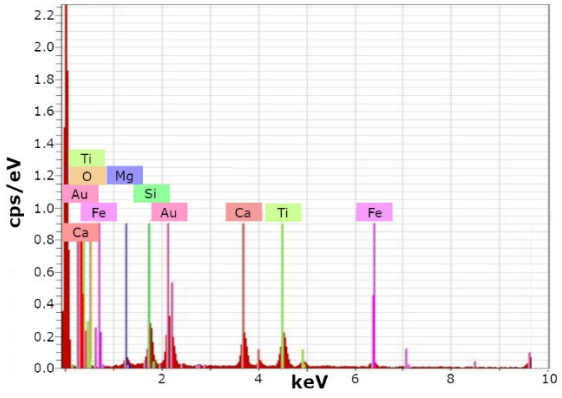

Fig. 4 Commercial anticorrosive EDX.

Table 3. Chemical composition of commercial anticorrosive.

Element	Chemical composition (wt %)
Ti	32.15
Si	18.75
Ca	18.71
O	17.99
Mg	7.58
Fe	4.82

The EDX of the commercial anticorrosive exhibits signals for Ti, Mg, O, Si, and Ca, which shows a composition very different from the NiO-ZrO_2Y used in the present investigation. The results can be seen in Fig. 4 and Table 3. The chemical composition suggests a mixture of Ti, Mg, Si, and Ca oxides. The Au signals are generated during the metallization of the film by the nanometric layer of gold deposited to make the film conductive.

3.2 Weight loss study

To simulate an accelerated corrosion process in a marine environment, bare steel and coated specimens were subjected to corrosion by immersion in 3.5% sodium chloride solution at a temperature of 29 °C with constant stirring at 7 rpm. The results show a constant weight loss in the uncoated HR steel, as can be seen by the green trend line of Fig. 5, showing that the weight loss is a direct function of the exposure time to the corrosive electrolyte. This can be seen from the micrographs obtained via SEM of Fig. 6a and 6b, where the surface morphology of the unexposed HR steel shows generalized imperfections throughout the entire surface, mainly large micro-cracks (white arrows) that accelerate the corrosion process exerted by the electrolyte.

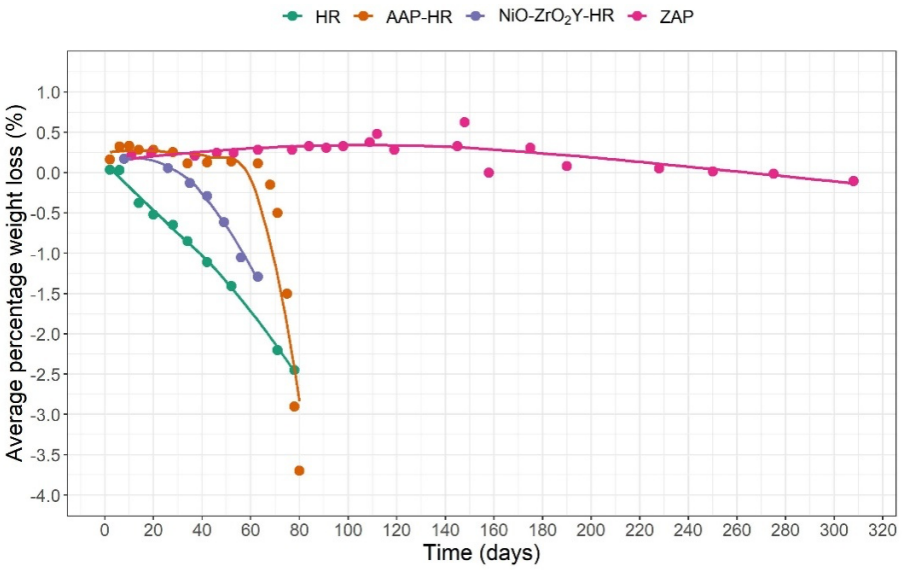

Fig. 5. Results of weight loss for the different coatings.

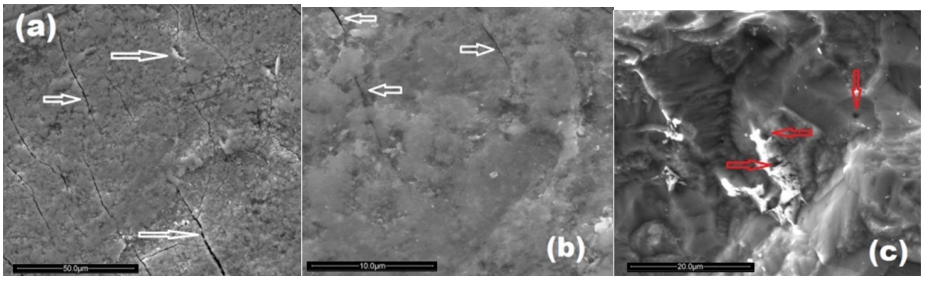

Fig. 6. SEM micrograph showing the morphology of HR steel after and before exposition to the 3.5% NaCl solution.

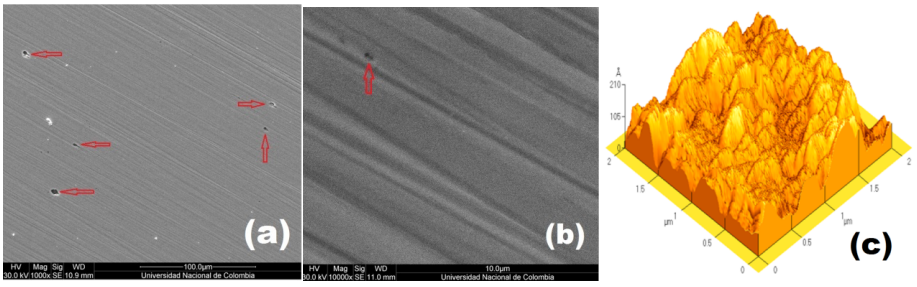

Fig. 7. SEM micrograph showing the morphology of the NiO-ZrO_2Y coatings

After 30 days of immersion in 3.5% NaCl solution, Fig. 6c, the scanning electron microscopy for the HR steel, the results of the weight loss give evidence of the corrosion process because of the change in the surface morphology of the samples subjected to immersion. Detachment of parts of the material caused by the oxidation of the iron to hydroxide can be seen, as presented in Equation 2. Additionally, micropores are generated by the surface loss of material, which contributes to the acceleration of the corrosion process (red arrow).

$$3Fe_{(s)} + 6H_2O_{(g)} \rightarrow 3Fe(OH)_{2(s)} + 3H_{2(g)} \quad (2)$$

The NiO_2-ZrO_2Y film is characterized by being highly homogeneous and exhibits the presence of micropores (red arrows), Fig. 7-a,b. The roughness evaluated using AFM was 3.23×10^{-3} μm with a particle size of 0.278μm, Fig. 7c. The NiO_2-ZrO_2Y film deposited on HR steel and exposed to immersion in NaCl solution exhibits an increase in weight during the first 12 days up to 0.2%, and subsequently starts its weight loss process at a rate lower than that of steel (Fig. 7 NiO_2-ZrO_2Y -HR). However, after 62 days of immersion, it reaches a weight loss of 2.5%, equal to that of uncoated steel.

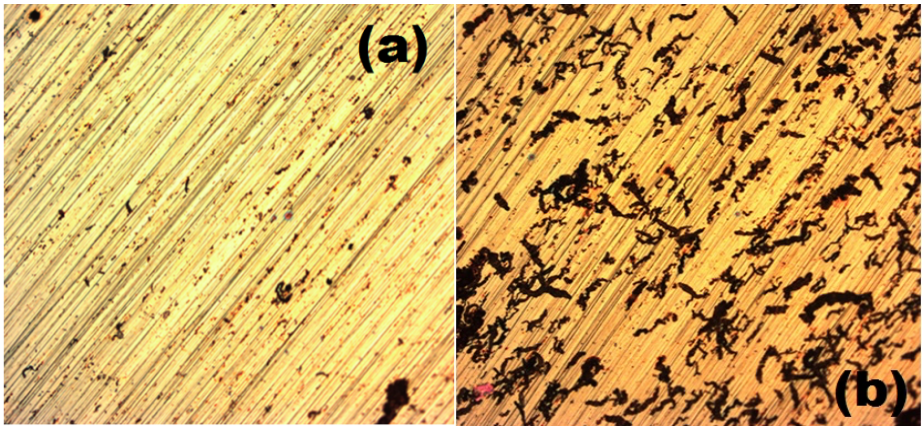

Fig. 8 Optical microscopy showing the migration of hydroxide through the pores of the NiO-ZrO_2Y coating.

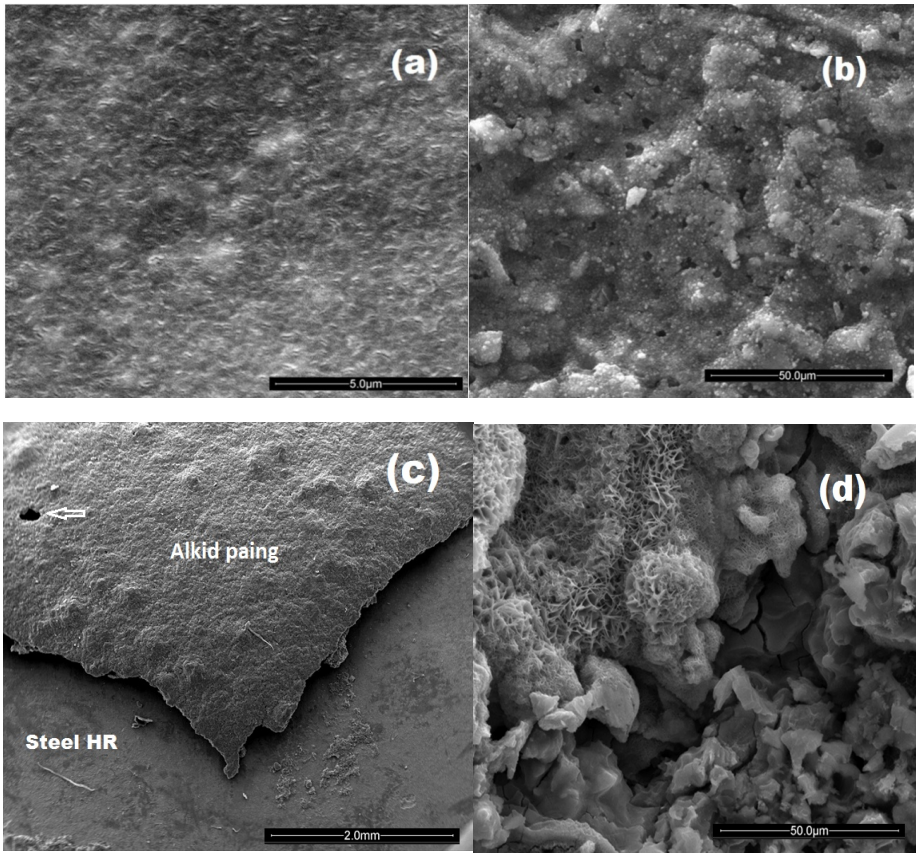

Fig. 9 SEM micrograph showing the morphology of the commercial anticorrosive-painting after 63 days of exposure to 3.5% NaCl solution.

The mechanisms by which the corrosion process of the NiO-ZrO_2Y-HR system occurs is probably an initial diffusion of the corrosive electrolyte through the pores of the coating, reaching the substrate. Once the iron oxidation begins, the hydroxide migrates through the pores of the coating and passes to the solution. This can be seen in the photograph of one of the samples shown in Fig. 8-a,b.

For the commercial anticorrosive-alkid painting system (AAP), green markers in Fig. 5, the specimens gain 0.3% in weight during the first month of exposure, then 30 days later the system stabilizes until day 63, when the coating's polymeric failure by delamination is seen in Fig. 9-c; hence the abrupt weight loss up to 3.7%. Comparing the morphology of the coating without exposure to the NaCl solution, Fig. 9-a, with the same after 30 days of immersion in NaCl solution, the microscopy shows that the alkyd paint has pores (Fig. 9-b), and therefore the increase in weight is attributed to the diffusion of the electrolyte through the polymer film, concentrating the solution under the polymer and generating a blister that breaks

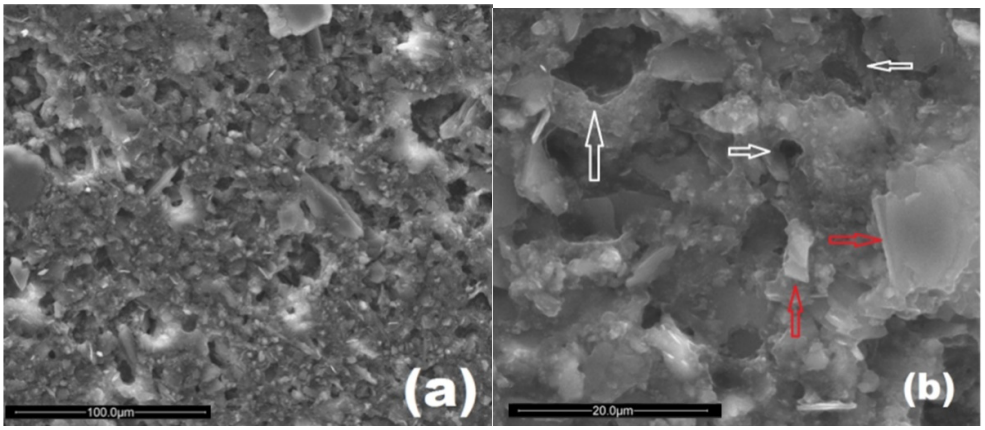

Fig. 10 SEM micrograph showing the morphology of the commercial anticorrosive after of exposure to the 3.5% NaCl solution.

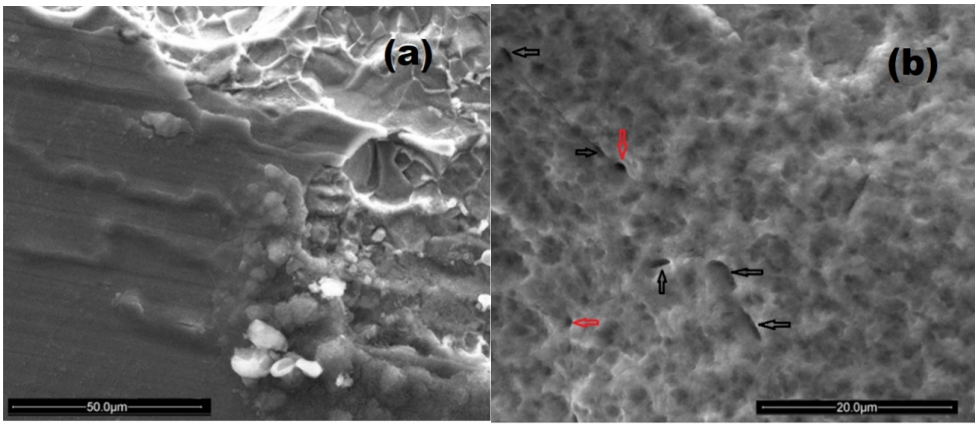

Fig. 11 SEM micrograph NiO-ZrO_2Ycoatings showing the morphology of the coatings after exposure to 3.5% NaCl solution.

and exposes the steel to the NaCl solution, with the subsequent accelerated corrosion process of the substrate, Fig. 9-d, which translates into a rapid weight loss, Fig. 5.

For the alkid painting-NiO-ZrO_2Y-HR system (ZAP-HR), the initial behavior is similar to that of the AAP-HR, an increase in average weight up to 0.35% up to day 30, when the system stabilizes, keeping the weight constant until day 150, when the weight loss process starts, ending at 304 days due to detachment of the alkyd paint layer. In both cases, the weight loss is due to delamination of the AP of the anticorrosive buffer layer or the NiO-ZrO_2Y film. While in the AAP-HR system the delamination process is rapid, with large fragments of AP, in the alkid painting-NiO-ZrO_2Y-HR system, the process is much slower, as can be seen by the change in weight recorded from day 150 to day 304. The NiO-ZrO_2Y coating increases the time by 75% of that of the coating before the corrosive attack.

The surface morphology after the immersion corrosion process shows that the degradation of the commercial anticorrosive is caused by delamination of the material (red arrow), with the formation of large micropores in a range of 2.0 to 8.0 μm (white arrows), Fig. 10-a,b. This makes the polymer film detach very quickly, because of the absence of anticorrosive-alkyd paining interaction forces. When a film of NiO-ZrO_2Y is used as a buffer layer between the steel and the alkyd paint, it is a homogeneous and uniform film (Fig. 7). Detachment of the film is observed due to the interaction with the corrosive electrolyte, Fig. 11-a, but there is no total loss, Fig. 11-b. The interaction forces of the coating-alkyd paint are much stronger, and the rupture process occurs more slowly. After immersion, a uniform degradation of the surface can be seen, with micropores in a range of 1.0 to 4.0 μm; therefore, the immersion time in the alkyd paint-NiO-ZrO_2Y-HR system was higher by 75% in comparison with the HR-anticorrosive-alkyd paint system traditionally used domestically.

3.2.1 FTIR AAP and ZAP-HR system

In order to demonstrate the changes in the structure of the anticorrosive-alkyd paint (AAP) and the alkyd paint -NiO-ZrO_2Y-HR (ZAP), the FTIR spectrum was recorded before and after the corrosion process in

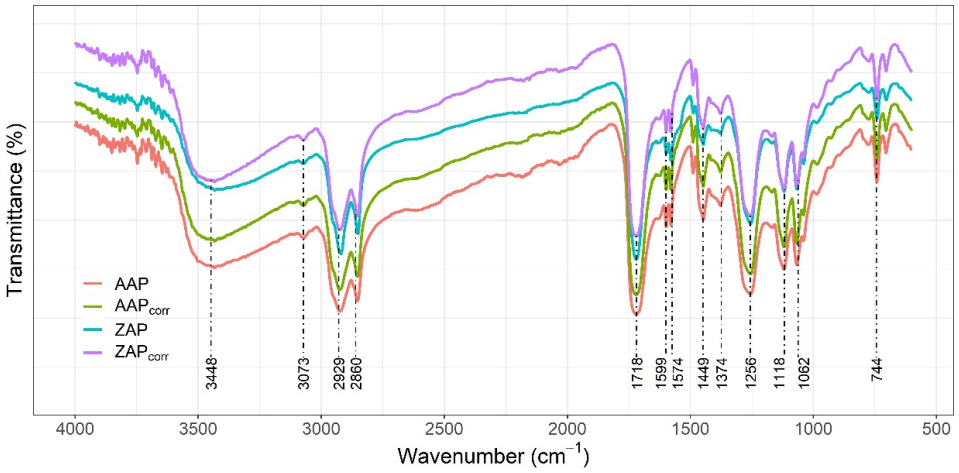

Fig. 12 FTIR spectrum of anticorrosive and alkid paint before and after corrosion.

NaCl solution after the failure of the specimen. The results obtained for the two systems studied via IR are identical. Those for the alkyd paint-anticorrosive-HR system and the ZAP-HR system are presented here. The characteristic bands of the spectra are presented in Fig. 12 and are described as follows: The broad singlet peaks at 3410 and 3448 cm^{-1} confirm the presence of the OH group (Flores *et al*., 2019; Hadzich *et al*., 2020), and the peak at 3073 cm^{-1} in Fig.12 corresponds to the mixture of oxides that make up the commercial anticorrosive (Nurtay *et al*., 2017). Peaks between 2931-2857 cm^{-1} are related to aliphatic C-H stretching vibration.

The stretching vibration of the carbonyl group, C=O, appears at 1718 cm^{-1}. Peaks at 1599 cm^{-1} and 1574 cm^{-1} correspond to C-C stretching vibration of aliphatic and aromatic C=C bands, respectively, while peaks around 1256-1062 cm^{-1} are related to stretching C-O-C vibrations(Hadzich *et al*., 2020; Nosal *et al*., 2016). The peak at 971 cm^{-1} is due to C-C stretching vibration, whereas out of plane aromatic C-H bending vibration is observed at 742.6-710 cm^{-1} (Chiplunkar & Pratap, 2016; Hadzich *et al*., 2020).

The results of the corrosion accelerated by immersion show that the alkyd paint layer does not undergo any degradation and that the failure of the commercial anticorrosive-paint specimen is due to loss of adherence of the paint to the commercial anticorrosive. When the porous layer of NiO-ZrO_2Y is used, it increases the corrosion resistance of the alkyd paint film, and its porosity favors the coating-substrate adherence, Fig. 13. Alkyd paint has poor interaction with steel, and the oxide layer used as a commercial anticorrosive did not prove to be very efficient as a buffer layer. However, if the anticorrosive traditionally used is replaced by NiO-ZrO_2Y, the adhesion, and therefore the corrosion resistance of the paint, increases.

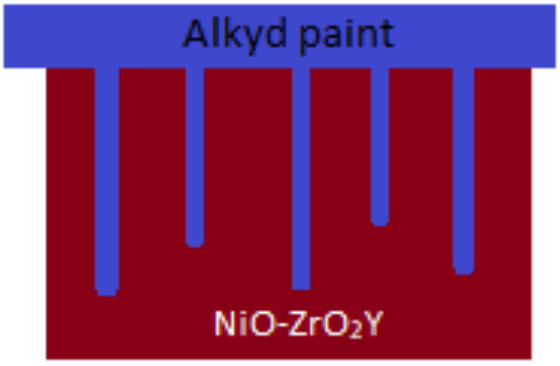

Fig. 13 Schematic representation of the NiO-ZrO_2Y-alkyd paint interaction.

3.3 Evaluation of corrosion resistance

3.3.1 Via electrochemical impedance spectroscopy (EIS)

The electrochemical impedance spectroscopy (EIS) study of HR steel provides information related to uncoated steel, of the paint applied on the commercial anticorrosive and of the paint applied on the coating NiO-ZrO_2Y, in order to evaluate their corrosion behavior. The results obtained after exposure to the corrosive action of a 3.5 wt. % NaCl solution for different immersion times are shown here: 1 h and 8, 15 and 30 days, in Fig. 14. The same color reference is used for the sample: red for HR, green for AAP-HR and blue for alkyd paint-NiO-ZrO_2Y-HR. In Fig. 14a are shown of Nyquist and Fig. 14b-c Bode plot, after different exposure times to the corrosive electrolyte.

After one hour of exposure to the corrosive electrolyte in Fig. 14-a, the increase in the diameter of the semicircle for Nyquist plot (log(|Z"|) vs log (|Z´|)) indicates a higher capacitive response for the AAP system compared to the ZAP. Bode plot (log |Z| vs. log frequency) shows that the magnitude of the impedance modulus is higher by six orders of magnitude for alkyd

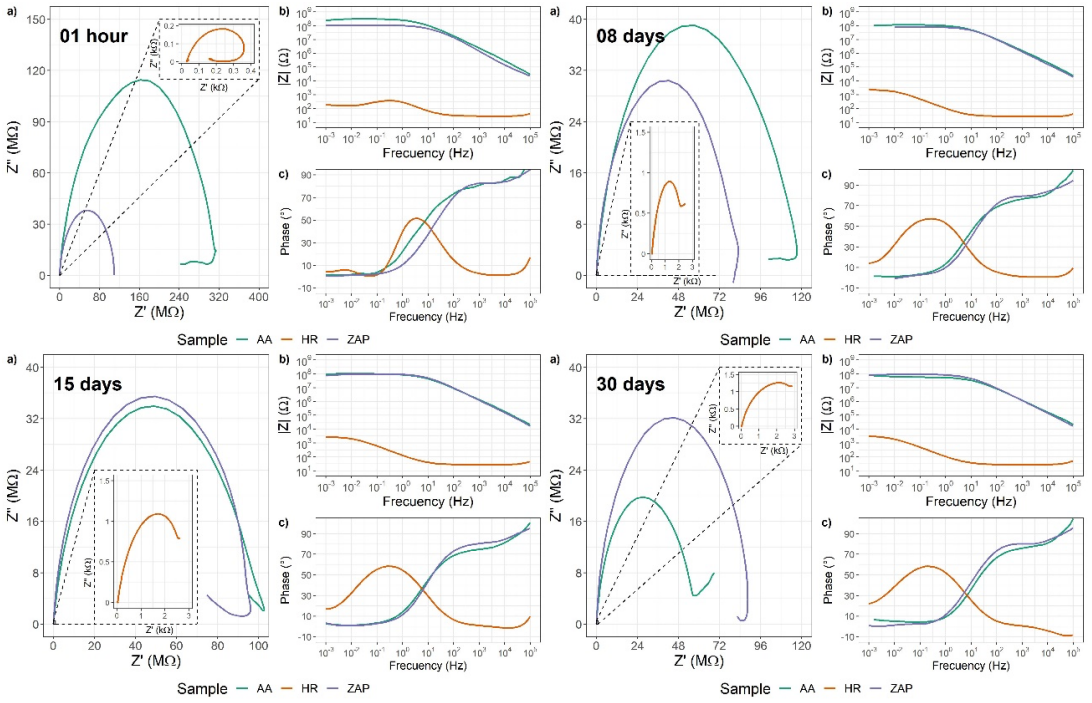

Fig. 14. Nyquist and Bode plots of HR, APP, NiO-ZrO$_2$Y-HR and ZAP samples.

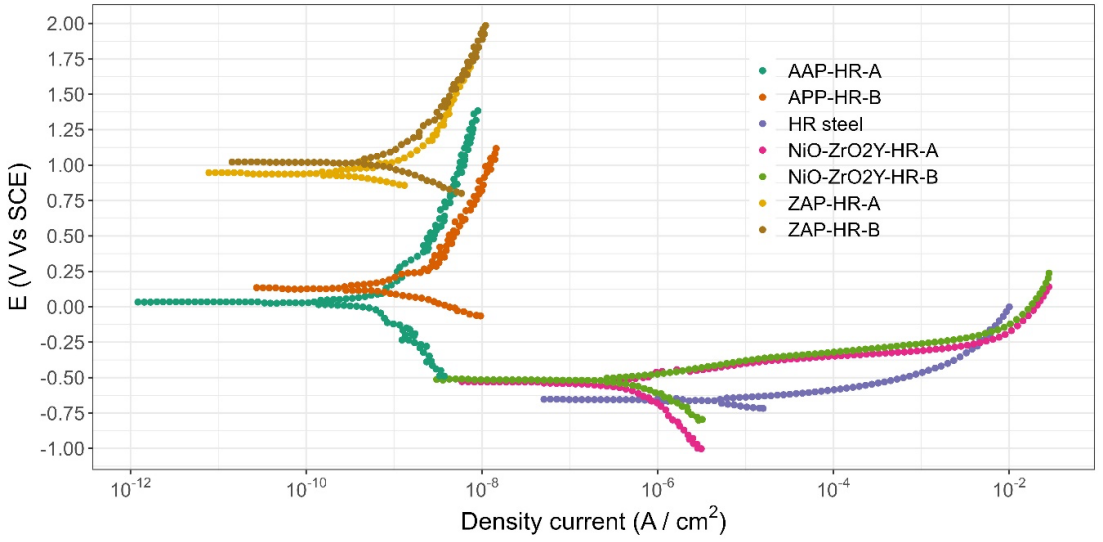

Fig. 15. Polarization curves of coatings and bare steel. A duplicate is presented in each case.

coated HR compared to bare steel. Between the two systems AAP and ZAP the change in the impedance modulus is not significant and the phase angle in the latter two is characterized by a large of plateau zone four orders of magnitude of frequency of (10^{-3} – 10^{5} Hz), being the phase angle 30° higher than steel. The displacement in four orders of magnitude towards high frequencies shows the higher capacitive response of the alkyd paint compared to HR steel.

As the exposure time increases, it is observed in Nyquist plot that the amplitude of the semicircle in AAP decreases, being approximately of the same order what ZAP after 15 days of exposure and lower with respect to ZAP after 30 days of exposure, which shows chemical changes in the coating and could be associated with a loss of corrosion resistance. However, the Bode diagram, Figs. 14b and c, shows that the impedance and the phase angle do not undergo significant variations, which indicates little degradation of the coating as a function of immersion time. This loss in the corrosion resistance of AAP is associated with the appearance of micropores in the paint film (see Fig. 9). ZAP shows no appreciable change in Nyquist plot during the exposure time. In general, Bode plot for AAP-HR and ZAP-HR as a function of exposure time shows no appreciable

Table 4 Results of the Corrosion Test.

Sample	J_{corr}(nA/cm^2)	E_{corr}(mV)	R_p (MΩcm^2)	CR(mmPY)
HR	11100	-651	0.0606	8.63×10^{-2}
NiO-ZrO_2Y-HR(a)	429	-514	0.0424	3.33×10^{-3}
NiO-ZrO_2YN-HR(b)	522	-514	0.0498	4.05×10^{-3}
AAP-HR(a)	0.264	28.0	98.5	2.05×10^{-6}
AAP-HR(b)	0.800	122	83.3	4.67×10^{-6}
ZAP-HR(a)	0.356	944	73.1 2.76×10^{-6}	
ZAP-HR(b)	0.589	904	59.3	4.21×10^{-6}

changes in impedance modulus and phase angle during the 30 days, since in both cases the corrosive electrolyte is directly in contact with the alkyd paint and not with the NiO-ZrO_2Y-HR or anticorrosive-HR interface.

3.3.2 Via potentiodynamic polarization

The corrosion potentials (E_{corr}) and the corrosion current density (J_{corr}) for the two coating-steel systems and for the steel without coating were determined from the polarization curves (Fig. 15). The results obtained are presented in Table 4. Despite being a porous coating, NiO-ZrO_2Y decreases the corrosion current density by an order of magnitude with respect to the bare steel, showing its ability to protect steel against corrosion. For the AAP and ZAP systems, a shift in J_{corr} towards lower values by approximately three orders of magnitude can be seen compared to the uncoated steel, which shows that the two coatings protect the steel against corrosion; however, the corrosion potential for the ZAP system is higher by 1.0 V compared to the AAP, showing a higher degree of steel protection for the ZAP system.

While it is true that the results obtained on the basis of the polarization curves do not show any significant difference in the corrosion current density compared to the AAP-HR system, with ZAP-HR system, the study of the corrosion on immersion in the 3.5% NaCl solution shows that the NiO-ZrO_2Y film, in comparison with the commercial anticorrosive-AP system, increases by 75% the time of contact of immersion in the corrosive electrolyte before failure because of low adherence to the substrate.

Conclusions

To improve the corrosion resistance of alkyd paints traditionally destined for domestic use, an NiO-ZrO_2Y thin film was deposited, replacing the commercial anticorrosive. The results obtained showed that the failure of the protection against corrosion of the alkyd paint occurs due to the generation of pores in it, allowing penetration of the corrosive electrolyte through them and detachment of the paint from the substrate. Compared with the anticorrosive used commercially, the NiO-ZrO_2Y film increases the corrosion resistance of the material subjected to immersion in the corrosive electrolyte by a factor of four.

Using XRD, it was found that the crystalline phases present in the NiO-ZrO_2Y film are: Y_2O_3-*c*, ZrO_2-c, NiO-c, and Fe_2O_3-c maghemite. Regarding its morphology, it is a highly porous, homogeneous film. The electrochemical and weight loss results indicate that this porosity favors the anchoring of the paint to the substrate, showing that NiO-ZrO_2 is a more efficient anticorrosive for protecting HR steel in a corrosive medium, as can be seen from the measurements of the corrosion tests by immersion and polarization.

Acknowledgment

This research was supported by the Asociación de Universidades Iberoamericanas and Universidad Nacional de Colombia Proyect HERMES 58935 and Laboratorio NA XPS Sede de Investigación Universitaria SIU Universidad de Antioquia.

References

Abdrabo, M. A., Abdelwahab, R. G., & Hassaan, M. A. (2022). Urban dynamics and potential vulnerability of coastal urban areas to sea level rise in the southeastern Levantine Basin. *Urban Climate 44*, 101212. https://doi.org/10.1016/j.uclim.2022.101212

Alonso-Villar, E. M., Rivas, T., & Pozo-Antonio, J. S. (2021). Resistance to artificial daylight of paints used in urban artworks. Influence of paint composition and substrate. *Progress in Organic Coatings 154*, 106180. https://doi.org/10.1016/J.PORGCOAT.2021.106180

Araujo, W. S., Margarit, I. C. P., Mattos, O. R., Fragata, F. L., & De Lima-Neto, P. (2010). Corrosion aspects of alkyd paints modified with linseed and soy oils. *Electrochimica*

Acta 55(21), 6204-6211. https://doi.org/10.1016/J.ELECTACTA.2010.03.088

Asemani, H. R., Ahmadi, P., Sarabi, A. A., &EivazMohammadloo, H. (2016). Effect of zirconium conversion coating: Adhesion and anti-corrosion properties of epoxy organic coating containing zinc aluminum polyphosphate (ZAPP) pigment on carbon mild steel. *Progress in Organic Coatings 94*, 18-27. https://doi.org/10.1016/J.PORGCOAT.2016.01.015

Barot, R. S., Patel, P., Patel, A., & Patel, A. (2020). Corrosion prevention and industrial economic analysis aspects for water heater. *Materials Today: Proceedings 28*, 1795-1800. https://doi.org/10.1016/j.matpr.2020.05.196

Bernasik, A., Kowalski, K., & Sadowski, A. (2002). Surface segregation in yttria-stabilized zirconia by means of angle resolved X-ray photoelectron spectroscopy. *Journal of Physics and Chemistry of Solids 63*(2), 233-239. https://doi.org/10.1016/S0022-3697(01)00135-4

Chen, C., He, Y., Xiao, G., Wu, Y., He, Z., & Zhong, F. (2018). Zirconia doped in carbon fiber by electrospinning method and improve the mechanical properties and corrosion resistance of epoxy. *Progress in Organic Coatings 125*, 420-431. https://doi.org/10.1016/J.PORGCOAT.2018.09.027

Chiplunkar, P. P., & Pratap, A. P. (2016). Utilization of sunflower acid oil for synthesis of alkyd resin. *Progress in Organic Coatings 93*, 61-67. https://doi.org/10.1016/J.PORGCOAT.2016.01.002

Cubillos, G. I., Romero, E., & Umaña-Perez, A. (2021). ZrN-ZrOxNy vs ZrO_2-ZrOxNy coatings deposited via unbalanced DC magnetron sputtering. *Scientific Reports 2021 11*(1), 1-19. https://doi.org/10.1038/s41598-021-98052-2

Escobar-Martinez, A., Vlasova, M., Márquez-Aguilar, P. A., Kakazey, M., & Guardián-Tapia, R. (2017). Transformación de la capa superficial de cerámica con tratamiento láser. *Revista Mexicana de Ingeniería Química 16*(2),591-603 https://www.redalyc.org/articulo.oa?id=62052087023

Flores, S., Flores, A., Calderón, C., &Obregón, D. (2019). Synthesis and characterization of sachainchi (*Plukenetiavolubilis* L.) oil-based alkyd resin. *Progress in Organic Coatings 136*, 105289. https://doi.org/10.1016/J.PORGCOAT.2019.105289

Gan, X., Yu, Z., Yuan, K., Xu, C., Zhang, G., Wang, X., Zhu, L., & Xu, D. (2018). Effects of cerium addition on the microstructure, mechanical properties and thermal conductivity of YSZ fibers. *Ceramics International 44*(6), 7077-7083. https://doi.org/10.1016/J.CERAMINT.2018.01.145

Hadzich, A., Gross, G. A., Leimbach, M., Ispas, A., Bund, A., & Flores, S. (2020). Effect of polyalcohols on the anticorrosive behaviour of alkyd coatings prepared with drying oils. *Progress in Organic Coatings 145*, 105671. https://doi.org/10.1016/J.PORGCOAT.2020.105671

He, Y., Zhang, S., He, Y., Song, R., Zhang, Z., Liu, B., Li, H., & Shangguan, J. (2022). Effects of yttrium-stabilized zirconia (different yttrium content) doping on the structure, corrosion resistance and wear resistance of Ni-P electroless coating. *Colloids and Surfaces A: Physicochemical and Engineering Aspects 654*, 130059. https://doi.org/10.1016/J.COLSURFA.2022.130059

International Organization for Standardization. (2019). Paints and varnishes-Corrosion protection of steel structures by protective paint systems-Part 5: Protective paint systems (Vol. 2019).

Jin, X., Bi, W., Wang, L., & Qian, H. (2020). Root cause analysis of pinhole defects on painted galvanized steel panel. *Engineering Failure Analysis 115*, 104598. https://doi.org/10.1016/J.ENGFAILANAL.2020.104598

Joos, J., Ender, M., Rotscholl, I., Menzler, N. H., & Ivers-Tiffée, E. (2014). Quantification of double-layer Ni/YSZ fuel cell anodes from focused ion beam tomography data. *Journal of Power Sources 246*, 819-830. https://doi.org/10.1016/J.JPOWSOUR.2013.08.021

Kausley, S. B., Desai, K. S., Shrivastava, S., Shah, P. R., Patil, B. R., & Pandit, A. B. (2018). Mineralization of alkyd resin wastewater: Feasibility of different advanced oxidation processes. *Journal of Environmental Chemical Engineering 6*(3), 3690-3701. https://doi.org/10.1016/j.jece.2017.04.001

Lei, P., Dai, B., Zhu, J., Tian, G., Chen, X., Wang, Y., Zhu, Y., Liu, G., Yang, L., & Han, J. (2015). Interfacial composition and adhesion of sputtered-Y_2O_3 film on ZnS substrate. *Applied Surface Science 351*, 119-124. https://doi.org/10.1016/J.APSUSC.2015.05.109

Lei, P., Zhu, J., Zhu, Y., Jiang, C., & Yin, X. (2013). Evolution of composition, microstructure and optical properties of yttrium oxide thin films with substrate temperature. *Surface and Coatings Technology 229*, 226-230. https://doi.org/10.1016/J.SURFCOAT.2012.03.074

Marsh, J., Scantlebury, J. D., & Lyon, S. B. (2001). The effect of surface/primer treatments on the performance of alkyd coated steel. *Corrosion Science 43*(5), 829-852. https://doi.org/10.1016/S0010-938X(00)00070-6

Mehvar, S., Filatova, T., Syukri, I., Dastgheib, A., & Ranasinghe, R. (2018). Developing a framework to quantify potential sea level rise-driven environmental losses: A case study in Semarang coastal area, Indonesia. *Environmental Science & Policy 89*, 216-230. https://doi.org/10.1016/j.envsci.2018.06.019

Nosal, H., Nowicki, J., Warzawa, M., Semeniuk, I., & Sabura, E. (2016). Synthesis and characterization of alkyd resins based on Camelina sativa oil, glycerol and selected epoxidized vegetable oils as functional modifiers. *Progress in Organic Coatings 101*, 553-568. https://doi.org/10.1016/J.PORGCOAT.2016.10.003

Nurtay, M., Tuersun, M., Cai, Y., Açkgöz, M., Wang, H., Pan, Y., Zhang, X., & Ma, X. (2017). Spectroscopic study for a chromium-adsorbed montmorillonite. *Spectrochimica Acta Part A: Molecular and Biomolecular Spectroscopy 173*, 114-121. https://doi.org/10.1016/J.SAA.2016.08.045

Roa, J. J., Laguna-Bercero, M. A., Larrea, A., Orera, V. M., & Segarra, M. (2011). Mechanical properties of highly textured porous Ni-YSZ and Co-YSZ cermets produced from directionally solidified eutectics. *Ceramics International 37*(8), 3123-3131. https://doi.org/10.1016/J.CERAMINT.2011.05.051

Shekari, E., Khan, F., & Ahmed, S. (2017). Economic risk analysis of pitting corrosion in process facilities. *International Journal of Pressure Vessels and Piping 157*, 51-62. https://doi.org/10.1016/j.ijpvp.2017.08.005

Talebi, T., Sarrafi, M. H., Haji, M., Raissi, B., &Maghsoudipour, A. (2010). Investigation on microstructures of NiO-YSZ composite and Ni-YSZ cermet for SOFCs. *International Journal of Hydrogen Energy 35*(17), 9440-9447. https://doi.org/10.1016/J.IJHYDENE.2010.04.156

Tansel, B., & Zhang, K. (2022). Effects of saltwater intrusion and sea level rise on aging and corrosion rates of iron pipes in water distribution and wastewater collection systems in coastal areas. *Journal of Environmental Management 315*, 115153. https://doi.org/10.1016/j.jenvman.2022.115153

Tripathi, P., Katiyar, P. K., Ramkumar, J., & Balani, K. (2020). Synergistic role of carbon nanotube and yttria stabilised zirconia reinforcement on wear and corrosion resistance of Cr-based nano-composite coatings. *Surface and Coatings Technology 385*, 125381. https://doi.org/10.1016/J.SURFCOAT.2020.125381

Turner, N. H., Ramaker, D. E., & Hutson, F. L. (1993). Accurate determination of Auger line shape binding energies. *Journal of Electron Spectroscopy and Related Phenomena 63*(2), 117-130. https://doi.org/10.1016/0368-2048(93)80043-L

Usseglio-Viretta, F., Laurencin, J., Delette, G., Villanova, J., Cloetens, P., & Leguillon, D. (2014). Quantitative microstructure characterization of a Ni-YSZ bi-layer coupled with simulated electrode polarisation. *Journal of Power Sources 256*, 394-403. https://doi.org/10.1016/J.JPOWSOUR.2014.01.094

Vorobel, R., Ivasenko, I., Berehulyak, O., &Mandzii, T. (2021). Segmentation of rust defects on painted steel surfaces by intelligent image analysis. *Automation in Construction 123*, 103515. https://doi.org/10.1016/J.AUTCON.2020.103515

Zhang, X., Chen, Z., Luo, H., Zhou, T., Zhao, Y., & Ling, Z. (2022). Corrosion resistances of metallic materials in environments containing chloride ions: A review. *Transactions of Nonferrous Metals Society of China 32*(2), 377-410. https://doi.org/10.1016/S1003-6326(22)65802-3

Zhang, Y., Ayyub, B. M., & Fung, J. F. (2022). Projections of corrosion and deterioration of infrastructure in United States coasts under a changing climate. *Resilient Cities and Structures 1*(1), 98-109. https://doi.org/10.1016/j.rcns.2022.04.004